Pinning effects in ceramic SmO$_{1-x}$F$_x$FeAs as revealed by microwave absorption

Nadezda Yu. Panarina,[*] Yurii I. Talanov, Tatyana S. Shaposhnikova, Niyaz R. Beysengulov, and Evgenia Vavilova

Zavoisky Physical-Technical Institute, Kazan 420029, Russian Federation

Günter Behr, Agnieszka Kondrat, Christian Hess, Norman Leps, Sabine Wurmehl, Rüdiger Klingeler, Vladislav Kataev, and Bernd Büchner

Leibniz Institute for Solid State and Materials Research, IFW Dresden, D-01171 Dresden, Germany

Modulated microwave absorption (MMA) measurements have revealed strong pinning of vortices in ceramic superconducting SmO$_{1-x}$F$_x$FeAs compounds with $x=0.06$, 0.08, and 0.1. Different behavior of MMA in small and strong fields enables to discriminate between intergranular and intragranular effects. Irreversibility lines due to the intragranular pinning exhibit a steep ascent comparable with that of the YBa$_2$Cu$_3$O$_7$ ceramics which is known to possess the highest pinning strength among cuprate high-temperature superconductors. A weak dependence of the critical current density on the magnetic field in the underdoped samples ($x=0.06,0.08$) indicates the presence of additional pinning centers. The analysis of the data together with the theoretical modeling yields a conclusion that strong pinning in SmO$_{1-x}$F$_x$FeAs is due to nonsuperconducting regions intermixed on a nanoscale with the superconducting phase.

PACS number(s): 74.70.Xa, 74.25.N−, 74.25.Wx, 74.25.Sv

I. INTRODUCTION

The recent discovery of a new class of high-temperature superconductors (HTSC) *Re*FeAsO (*Re* =Sm,Nd,Pr,Ce,La) (Ref. 1) has generated considerable excitement in the scientific community. The interest to oxypnictides is attracted by the fact that superconductivity arises in the planes containing iron ions but not copper as in cuprate HTSC materials and that the parent undoped material is an antiferromagnetic metal and not a Mott-Hubbard insulator. A comparative analysis of superconducting properties of pnictides and cuprates may be helpful in clarifying the origin of high-temperature superconductivity. Furthermore, understanding of the unusual properties of the vortex matter in HTSC is of fundamental importance as well,[2] besides its relevance for technological applications. Among the pnictides known up to date, SmO$_{1-x}$F$_x$FeAs superconductors possess one of the highest critical temperatures T_c up to ∼55 K at optimal doping.[3,4] In this context, the superconducting characteristics of this "record" material, such as the critical current density j_c, as well as the irreversibility line $H_{irr}(T)$, which is the boundary between the states with zero and nonzero critical current density, take on particular significance. Since some of these parameters are affected by pinning, experimental insights into the origin and effectiveness of pinning centers in SmO$_{1-x}$F$_x$FeAs are important. In contrast to the La-based analog which shows a sharp first-order-like boundary that separates the antiferromagnetic spin-density-wave state at small fluorine doping and the superconducting state at larger doping levels,[5,6] in SmO$_{1-x}$F$_x$FeAs magnetic order and superconductivity can coexist in a certain range of fluorine doping (see, e.g., Ref. 7). Depending on the particular nature and length scale of the phase mixture, coexistence has clear implications for the pinning since inclusions of nonsuperconducting magnetic phase can serve as centers for vortex pinning, and one may expect the enhancement of the pinning strength.

In the present paper pinning effects in ceramic SmO$_{1-x}$F$_x$FeAs samples are studied with the help of the microwave absorption technique widely used before for studies of cuprate HTSC materials. The method relies on the dissipation of microwave power in superconducting samples by vibrating vortices and can give information about the pinning strength in the system (see, e.g., Ref. 8 and references therein). Our measurements of modulated microwave absorption (MMA) in the superconducting samples with different fluorine content in a broad temperature and magnetic field range with subsequent theoretical analysis enable the evaluation of the relevant superconducting parameters characterizing the vortex state of SmO$_{1-x}$F$_x$FeAs. Furthermore, we find strong experimental indications for enhanced pinning in the underdoped regime. This finding is suggestive of a nanoscale mixing of superconducting and normal state (possibly magnetic) phases and thus corroborates the growing evidence for the coexistence of the phases with competing order parameters in the underdoped Sm-based iron arsenide superconductor.

II. MATERIALS AND METHODS

Ceramic SmO$_{1-x}$F$_x$FeAs samples in the form of sintered dense pellets were prepared using a two-step solid-state-reaction method described elsewhere.[9] The composition of the synthesized samples was investigated by wavelength-dispersive x-ray (WDX) spectroscopy according to which the ratio of the actual to the nominal fluorine content is approximately 1:2.5. The doping levels x estimated by WDX amount to 0.06, 0.08, and 0.1 for the three SmO$_{1-x}$F$_x$FeAs samples under study. The high phase purity of the samples has been confirmed by x-ray diffraction. The analysis of the powder x-ray diffraction data reveals only a small amount of impurity phases, SmOF and FeAs, which appear in concentrations of about 4%. In order to determine the microstructure of the samples, scanning electron microscopy (SEM) has been applied. As an example, the SEM image and a histogram distribution of grain lateral dimensions for SmO$_{0.9}$F$_{0.1}$FeAs are
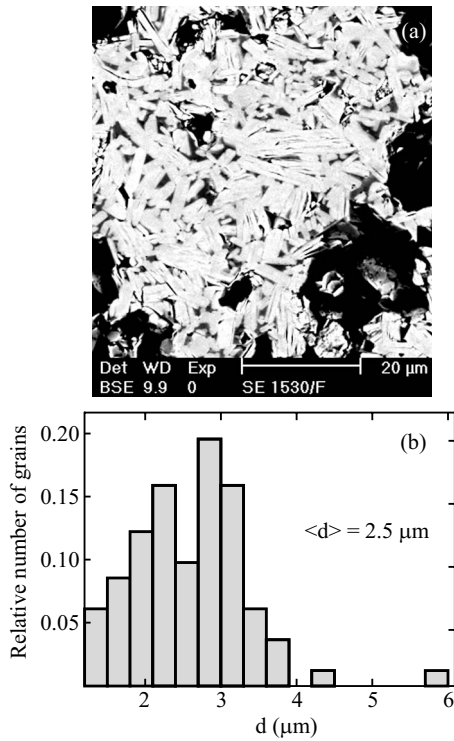
FIG. 1. (a) SEM image of a polycrystalline $SmO_{0.9}F_{0.1}FeAs$ sample. White stripes are the superconducting grains and black spots are voids. (b) Histogram distribution of lateral grain dimensions for the $SmO_{0.9}F_{0.1}FeAs$ sample. An average lateral dimension is 2.5 μm and the length of grains varies between 5–15 μm.

shown in Figs. 1(a) and 1(b), respectively. The samples exhibit well-connected stripelike grains of $SmO_{1-x}F_xFeAs$ with an average lateral dimension of about 2.5 μm and length of 5–15 μm. The morphology shown in Fig. 1 is similar for all samples under study.

The superconducting transition temperatures T_c were determined from standard resistivity, ac susceptibility and static magnetization measurements [Figs. 2(a)–2(c), respectively]. All methods give very close results of the critical temperature T_c=36, 44, and 53 K as determined at the half-height of the superconducting transition and the onset critical temperature T_c^{onset}=39, 49, and 55 K for the samples with the fluorine content x=0.06, 0.08, and 0.1, respectively. Our samples hence are in both optimal doping (x=0.1) and underdoped (x=0.06,0.08) superconducting regimes of the phase diagram.[4] The dc susceptibility $\chi(T)$ [Fig. 2(c)] has been measured in magnetic fields of 1 mT (x=0.08 and 0.1) and 2 mT (x=0.06), respectively, in which the $M(B)$ curve at low-temperature exhibits linear behavior. The data have been corrected for demagnetization effects. For the lowest doping level x=0.06, the susceptibility and resistivity (Fig. 2) demonstrate a rather sharp transition without any features. Upon further doping, at x=0.08, a step in $\chi(T)$ and resistivity data appears, and becomes even more pronounced and shifts to higher temperatures at x=0.1. As will be discussed below, the origin of this kink is connected with the granular structure of the sample.

Measurements of the modulated microwave absorption have been carried out on a standard x-band electron para-
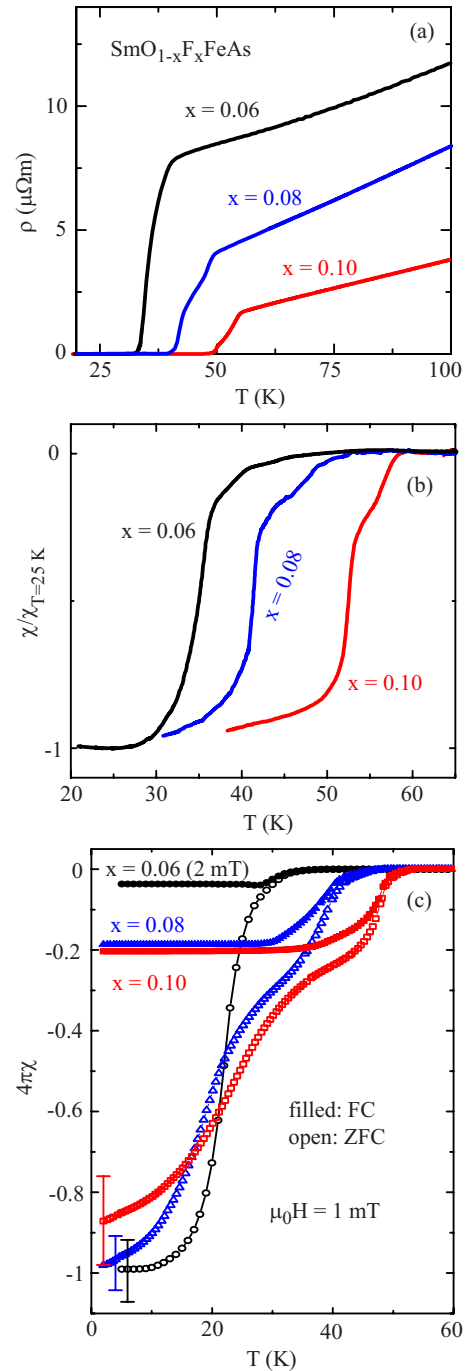

FIG. 2. (Color online) Superconducting transition temperatures of the $SmO_{1-x}F_xFeAs$ samples with different fluorine doping as determined from the temperature dependence of (a) resistivity, (b) ac susceptibility, and (c) static magnetization. Onset critical temperatures are 39, 49, and 55 K for the samples with the fluorine content x=0.06, 0.08, and 0.1, respectively. Error bars reflect the uncertainty of the estimation of the demagnetization factor and of the sample volume.

magnetic resonance (EPR) spectrometer with magnetic field modulation (100 kHz) of small amplitude (0.05 mT) and lock-in detection (see a brief description of the method below). In the experiment, a sealed sample was placed in a resonance cavity and cooled down to the measurement tem-

perature below the critical temperature in a remanent field of the magnet. A helium-flow cryostat was used for obtaining temperatures in the range of 10–60 K. At fixed temperatures, the magnetic field was swept up from about 6 mT to the value of about 0.7 T and then down to the initial value. The MMA hysteresis loops were registered in a wide temperature range and analyzed with the help of an appropriate theoretical model of microwave absorption.[10]

The distribution of the local magnetic field on the superconducting pellet surface was registered by a scanning Hall sensor. The magnetic flux profile was registered at different magnetic fields in the range from 3 mT to 0.2 T at temperatures below T_c.

Since exposure to air is known to deteriorate the superconducting properties of SmO$_{1-x}$F$_x$FeAs, in order to prevent degradation of the samples during experiments, the material was sealed in glass ampoules with pure helium gas. When contact with air was unavoidable during our studies of the magnetic-flux profile on the surface, the time of air exposure has been minimized to several minutes.

Modulated microwave absorption

The MMA method enables to study the modulated microwave absorption, which is determined by the number and the particular properties of vortices, such as viscosity of vortex matter and pinning strength. The distribution of vortices inside a type-II superconductor is inhomogeneous and depends on the number and strength of pinning centers present in the sample. In the case of an infinitely thin stripe oriented parallel to the magnetic field, the gradient of vortices can be described by a simple Bean's model.[11] For samples with finite dimensions in the perpendicular geometry, a more complicated distribution calculated by Brandt[12] is applicable. When a 9 GHz microwave field is applied to a superconductor, the vortices oscillate under the action of an alternating Lorentz force induced by the microwave current. This motion results in substantial dissipation of the microwave field power by nonsuperconducting cores of vortices. With the low-frequency modulation of the applied magnetic field, the induced current in each point of the sample is also modulated with the same frequency. So the absorbed power turns out to be modulated as well. This fact is reflected in the name of the method, modulated microwave absorption. A lock-in amplifier used for the detection of the signal extracts the fundamental harmonic of the absorption power on the modulation frequency. The detected signal depends on several parameters, such as the critical current density, the viscosity of the vortex matter, thermal fluctuations of the vortex position, instantaneous distributions of fields and induced currents (see Sec. IV). Upon reversal of the sweep direction of the applied field, the distribution of magnetic fields (gradient of vortices) and currents changes, and a hysteresis of the MMA is observed.

III. RESULTS OF MICROWAVE ABSORPTION MEASUREMENTS

MMA hysteresis loops have been measured in a wide range of magnetic fields and at different temperatures. Se-
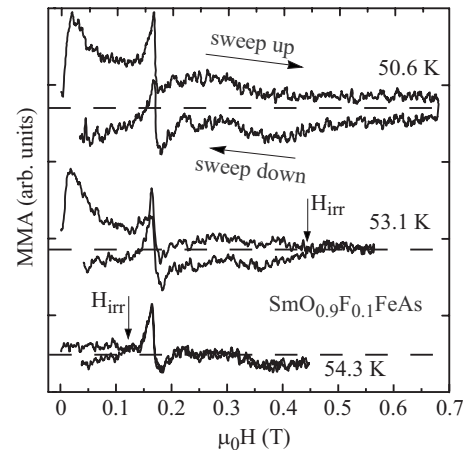

FIG. 3. Hysteresis loops recorded at different temperatures below T_c for a polycrystalline SmO$_{0.9}$F$_{0.1}$FeAs sample. Horizontal arrows show the sweep direction. Vertical arrows indicate the location of the irreversibility field H_{irr}. Dashed middle line indicates the constant, field-independent level of absorption.

lected curves are shown for SmO$_{0.9}$F$_{0.1}$FeAs in Fig. 3. Note that along with the MMA data, a spurious EPR signal from the sample container is observed at the magnetic field of around 0.16 T. The main feature in Fig. 3 is the evolution of a MMA hysteresis, i.e., a different MMA on up-sweeping and down-sweeping the magnetic field. The hysteresis is observed below the onset critical temperature of the superconducting transition. Its shape changes drastically on decreasing the temperature by a few kelvin. The MMA loops are almost symmetrical with respect to the horizontal axis just below T_c. In this temperature interval the irreversibility fields H_{irr} at which the hysteresis loops collapse are rather small. On further cooling the hysteresis loops become asymmetrical. This asymmetry is associated with the occurrence of the low-field peak (at magnetic fields below 0.1 T). The irreversible regime of the superconductor continuously expands to higher magnetic fields with decreasing temperature. Eventually, as exemplified by the data at T=50.6 K (Fig. 3), the irreversibility fields exceed the available magnetic fields of 0.7 T and cannot be registered anymore. It should be noted that this technique allows a registration of only the irreversible part of absorption. The reversible part of absorption, though present as a certain bias level, does not change upon reversing the field sweep direction and, therefore, it does not contribute to the MMA hysteresis. Therefore, the absolute zero level, which includes the level of reversible absorption, cannot be determined. A middle line is indicated in Figs. 3–5 and 7, which divides the hysteresis loop into two parts symmetrical at high magnetic fields and just serves as a guide to the eye.

The characteristic shape of the MMA loops measured at the field values well above the low-field peak differs from those shown in Fig. 3. A shape of the loop typical for a short sweep interval at high magnetic fields is shown in Fig. 4. The loop was registered around the magnetic field value of 0.25 T for the SmO$_{0.9}$F$_{0.1}$FeAs sample. In this experiment, the sample was cooled down to the temperature of the measurement below T_c and then a field of 0.245 T was applied. From
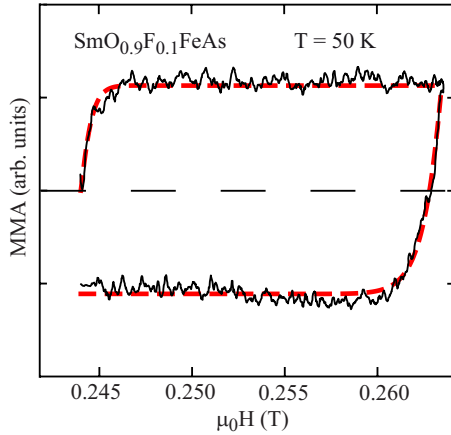
FIG. 4. (Color online) MMA hysteresis loop for the $SmO_{0.9}F_{0.1}FeAs$ sample recorded in the magnetic field around 0.25 T at $T=50$ K: solid line, experimental loop; dashed line, simulated loop. Long-dashed middle line indicates the constant, field-independent level of absorption.

this value the field was swept up by 15 mT and then down to the initial point. The achievement of the initial demagnetized state is not required for the MMA experiment since the reversible magnetization does not contribute to the MMA hysteresis loop. As one can see in Fig. 4, in this "high-field" regime there is no peak in the beginning of the hysteresis and the loop is symmetrical with respect to the horizontal axis. The data hence denote that the low-field peaks of the MMA hysteresis displayed in Fig. 3 are not related to the mechanism of the hysteresis loop formation at higher fields.

The shape of MMA hysteresis depends not only on the magnetic field but also changes with temperature. This is
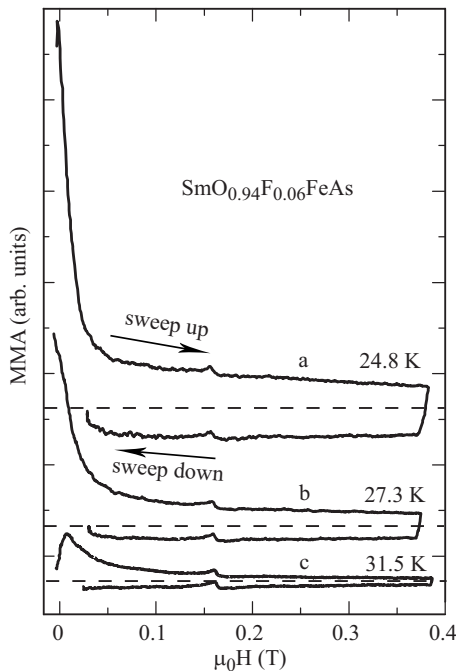

FIG. 5. MMA hysteresis loops recorded for the $SmO_{0.94}F_{0.06}FeAs$ sample at different temperatures: (a) $T=24.8$ K, (b) $T=27.3$ K, and (c) $T=31.5$ K. Dashed middle line indicates the constant, field-independent level of absorption.

shown in Fig. 5 which presents loops registered for $SmO_{0.94}F_{0.06}FeAs$ at different temperatures. The amplitude of the low-field peak grows drastically as the measurement temperature gradually decreases. The same tendency is observed for the amplitude of the MMA hysteresis at high magnetic fields. The narrow-neck behavior typical for ceramics, though in part visible in Figs. 5(a) and 5(b), is restricted to the low-field region, which is not covered experimentally due to the field delay upon the down-sweep. As will be shown below, analyzing the shape of the MMA loop, as well as its field and temperature dependences allows one to draw a conclusion about the pinning type (bulk or surface) dominating in the system. It should be noted that, though not shown in the figure, the MMA loops for $SmO_{0.92}F_{0.08}FeAs$ exhibit the same shape as for the other two samples and the amplitude of the low-field peak is intermediate between those of the two samples shown.

A spurious EPR signal at the resonance field of about 0.16 T, though undesired, enables tracking and eliminating the technical hysteresis of the spectrometer field unit due to magnetic field delay upon sweeping. Note, that in our high-quality samples we do not detect any intrinsic EPR signal related to Fe. The d electrons of these ions are delocalized in iron pnictides. Thus their momentum scattering should yield a very fast spin relaxation owing to a strong spin-orbit coupling and consequently a huge broadening of the EPR line. The recently reported EPR signals in La(O,F)FeAs are hence most likely of an extrinsic origin.[13]

Supplementary experiments on measuring the magnetic-flux profile on the sample surface with a scanning Hall sensor were carried out for the underdoped $SmO_{0.92}F_{0.08}FeAs$. They have shown the absence of the Bean distribution[10] over the whole of the sample. This implies that it takes place only on the size scale of the grains. Therefore, an average lateral dimension of individual grains, which was estimated to be 2.5 μm, was used in the calculations of the critical current density for the three samples under study, as discussed in the next section.

IV. DISCUSSION

The granular structure of the samples manifests itself in all experimental data. Superconducting grains are separated from each other by nonsuperconducting material of molecular thickness, which can form Josephson-type junctions between the grains. In particular, such weak junctions may explain the kinks in the superconducting transitions found in susceptibility and resistivity measurements (Fig. 2). Let us examine the temperature dependence of the dc susceptibility on zero-field cooling (ZFC). At low temperatures, the weak links between the grains contribute to superconductivity and provide superconducting paths for the Meissner shielding current across the whole sample. As the temperature increases, the weak links start breaking down due to a reduction in the Josephson critical field and the applied magnetic field starts to penetrate into the intergranular space of the sample. At temperatures close to T_c, i.e., where the susceptibility is above 2/3 of the complete diamagnetic signal, shielding currents flow within separate superconducting

grains. In case of field cooling (FC), the kink in the transition is also due to the establishment of intergranular links. Thus, the steplike feature in superconducting transitions is connected with a granular structure of the sample and originates from different shielding regimes in the sample. Similar conclusions have been made in Refs. 14–16. The absence of the kink in the superconducting transition for the sample with the lowest doping level $x=0.06$ may be due to larger nonsuperconducting inclusions between the superconducting grains, which prevent the formation of weak links. In agreement with the doping dependence of the ZFC data, the shielding signal as obtained from the FC measurements increases monotonously. We note here that an influence of the impurities on the superconducting transition is unlikely since the amount of foreign phases in the studied crystals is very small (see Sec. II).

In addition to causing a steplike feature in the ac susceptibility, the granularity also affects the pinning and, hence, the MMA data. At temperatures near the onset T_c, only intragranular pinning is present which results in symmetrical MMA hysteresis loops typical for bulk pinning[10] (see Fig. 3, $T=54.3$ K). The emergence of weak links of any nature leads to the appearance of vortices (both Abrikosov vortices and Josephson ones) that are pinned in the space between the grains. At a certain temperature below T_c (about 2/3 of the superconducting transition), the intergranular pinning of a surface type begins to contribute to the MMA hysteresis along with the bulk pinning inside the grains. This contribution results in the appearance of the low-field peak which renders the MMA loop asymmetrical (the absence of the peak on down-sweeping the magnetic field is due to the interruption of the magnetic field sweep at a finite field value). The fact that this peak is restricted to low fields results from a decrease in the intergranular pinning on breaking up the weak links as the magnetic field increases.[17] Our assumption of a contribution of Josephson vortices is supported by works of Pozek $et\ al.$,[18,19] where it has been shown that in ceramic samples a MMA hysteresis at low magnetic fields can be very well described by theoretical model involving Josephson weak links. This scenario straightforwardly explains the experimentally observed absence of the peak in the hysteresis loops registered in the magnetic field around 0.25 T (Fig. 4). Note that the amplitude of the low-field peak increases with decreasing temperature (Fig. 5). This tendency reflects the temperature dependence of the Josephson current between the grains, which increases at low temperatures.[17]

Along with the low-field peak originating from intergranular pinning, the MMA loop has symmetrical, slowly narrowing part. It is characterized by a hysteresis collapse at a certain value of the magnetic field depending on the measurement temperature. Such behavior can be explained by dependence of the MMA hysteresis on the value of the critical current density, which is a decreasing function of the magnetic field. As the critical current density becomes zero at some value of the magnetic field H_{irr}, the superconductor passes into the reversible regime. Since the hysteresis vanishes at fields higher than the location of the low-field peak, the irreversibility line of the sample $H_{irr}(T)$ is defined by pinning inside grains of the pellet.

Irreversibility fields H_{irr} as a function of temperature yield the irreversibility line $H_{irr}(T)$ that separates the areas with

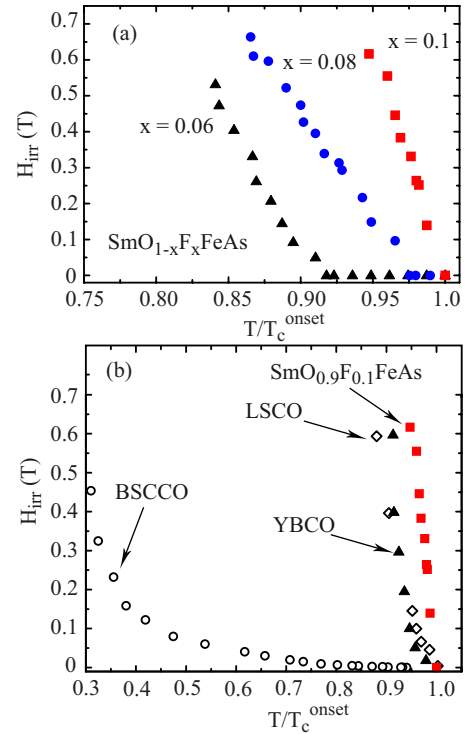FIG. 6. (Color online) (a) Irreversibility lines for SmO$_{1-x}$F$_x$FeAs samples reduced to the onset critical temperature: triangles, $x=0.06$; circles, $x=0.08$; and squares, $x=0.1$. (b) Irreversibility lines for polycrystalline HTSC compounds: squares, SmO$_{0.94}$F$_{0.06}$FeAs; triangles, YBCO (Ref. 21); diamonds, LSCO (Ref. 22); and circles, BSCCO (Ref. 23).

nonzero and zero critical current density on the phase diagram of magnetic fields and temperatures. The irreversibility lines for the samples with different fluorine content are presented in Fig. 6(a). In general, the position of irreversibility lines for underdoped samples ($x=0.06$ and 0.08) and optimally doped sample ($x=0.1$) on the plane of magnetic fields and temperatures is defined by their critical parameters, in particular, by the critical temperature T_c. Note that the irreversibility regime sets in at lower temperatures for samples with smaller T_c (lower fluorine content).

It is interesting to compare the irreversibility line of pnictides with those of cuprate high-temperature superconductors. Such a comparison of the SmO$_{0.9}$F$_{0.1}$FeAs sample with YBa$_2$Cu$_3$O$_7$ (YBCO), La$_{1.85}$Sr$_{0.15}$CuO$_4$ (LSCO), and Bi$_2$Sr$_2$CaCu$_2$O$_8$ (BSCCO) ceramics is shown in Fig. 6(b). Since all these compounds have different critical temperatures T_c, the comparison is drawn on a reduced temperature scale T/T_c. The samples being compared are ceramics unmodified by doping with artificial pinning centers, which are known to enhance pinning.[20] It is seen that the slope of the irreversibility line observed for pnictides is similar to and even sharper than that reported for YBCO samples.[21] YBCO compound possesses the maximum pinning strength among unmodified HTSC cuprates. Even LSCO samples[22] are characterized with a weaker dependence $H_{irr}(T)$ while the irreversibility line of BSCCO ceramics[23] is very flat, especially near T_c. The revealed tendency is indicative of a strong pinning in SmO$_{1-x}$F$_x$FeAs pnictides. It should be noted that
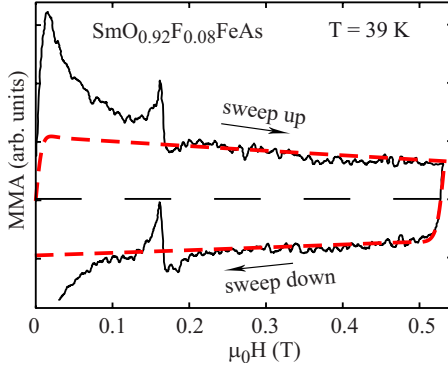
FIG. 7. (Color online) Experimental (solid line) and theoretical (dashed line) MMA hysteresis loops for the $SmO_{0.92}F_{0.08}FeAs$ sample at $T=39$ K. Long-dashed middle line indicates the constant, field-independent level of absorption.

similarity in superconducting parameters of pnictides and HTSC cuprates is also revealed in microwave surface impedance measurements by Narduzzo *et al.*[24]

From MMA measurements one can obtain further important characteristics of a superconductor, besides the irreversibility line. Before continuing the discussion of the data we note that the analysis of the intergranular pinning, which to a large extent is a sample-related property and contains little information about bulk superconducting parameters, is out of the scope of the present work. It yields at low fields a discrepancy between experimental curves and the model of the intragranular pinning to be discussed below. Hereafter we concentrate on the MMA response at higher magnetic fields which provides valuable information on the intrinsic characteristics of a superconducting material.

Generally, the MMA hysteresis is a complex function of the critical current density j_c, the viscosity of the vortex system η, the ratio of the amplitude of thermal fluctuations to the mean distance between pinning centers $\langle u^2\rangle/a^2$, and of the distribution of fields $H(r,t)$ and currents $j(r,t)$. In order to estimate these parameters an appropriate theoretical model is required as suggested by Kessler *et al.*[25] and developed by Shaposhnikova *et al.*[10,26] Within these approaches, an expression for the power absorbed by oscillating vortices upon sweeping the magnetic field can be obtained by solving the equation of motion of a flux line. We have applied the results of Refs. [10] and [26] for simulating the MMA hysteresis loops numerically. The results are shown by dashed lines in Figs. [4] and [7] . In Fig. [4] the model curve nicely fits the experimental data, i.e., the loop registered in a small magnetic field range at higher fields while in Fig. [7] there is a discrepancy between theoretical and experimental curves at low magnetic fields. This discrepancy can be attributed to the above-mentioned contribution of the intergranular pinning which is not considered in the theoretical model used, being valid only for bulk intragranular pinning.

In order to estimate the unknown superconducting parameters numerically, the temperature dependence of the microwave hysteresis amplitude L at a fixed magnetic field $H=0.2$ T plotted in Fig. [8] for the samples with different fluorine content has been analyzed. The amplitude of the microwave absorption hysteresis was determined from experimen-
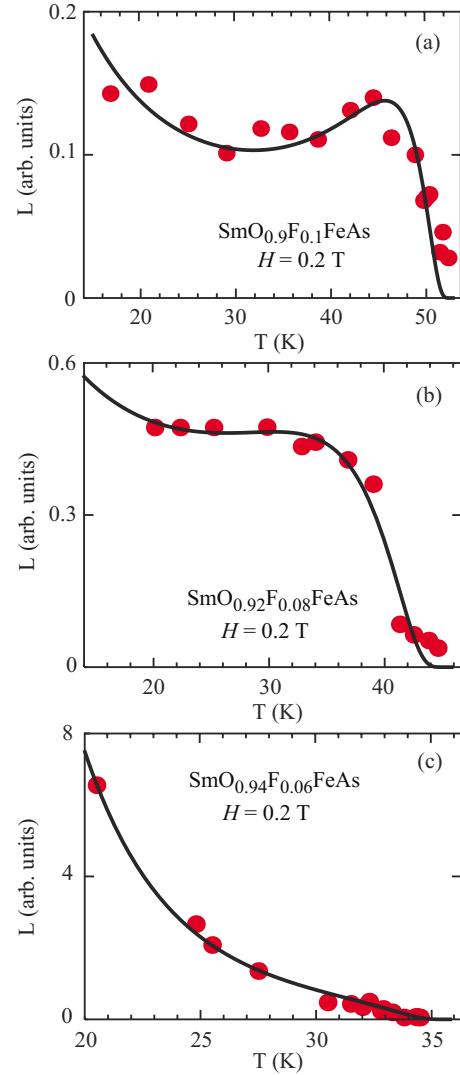

FIG. 8. (Color online) Temperature dependence of the MMA hysteresis amplitude at the applied magnetic field $H=0.2$ T for the $SmO_{1-x}F_xFeAs$ samples with different fluorine doping: (a) $x=0.1$, (b) $x=0.08$, and (c) $x=0.06$. Solid line is the result of numerical calculations, symbols are the experimental data.

tal MMA loops as the difference between magnitudes of the power absorbed upon sweeping the magnetic field up (P_{up}) and down (P_{down}). Theoretically the MMA hysteresis amplitude can be described with the following expression:[26]

$$L = P_{up} - P_{down} = A\frac{j_c^2(H,T)}{\eta^{7/2}(T)}\exp\left(-\frac{8\pi^2\langle u^2(T)\rangle}{a^2}\right)$$

$$\times[F_{up}(H,j,j_c) - F_{down}(H,j,j_c)], \qquad (1)$$

(1)where A is an instrument-dependent constant, and F_{up} and F_{down} are the integrals accounting for instantaneous distributions of field and current. The analytical expressions for F_{up} and F_{down} are given in Ref. [26] while the instantaneous distributions of the field and current used in calculations are taken from Ref. [11]. The integrals F_{up} and F_{down} containing the critical current density as a parameter determine the shape of the MMA loop while the coefficient before the in-

tegrals in square brackets define the magnitude of this loop. The model function Eq. (1) contains three parameters describing the properties of the superconducting state: the critical current density j_c, the ratio of the amplitude of thermal fluctuations u to the mean distance a between pinning centers ($\langle u^2 \rangle / a^2$), and the viscosity of the vortex matter η.

As can be seen from Fig. 8, the temperature dependence of the MMA amplitude is quite different for the three samples under study. For the SmO$_{0.9}$F$_{0.1}$FeAs sample, there is a local maximum near T=45 K, which disappears with decreasing fluorine concentration. Such behavior of $L(T,H$=const) may be described using temperature dependences of superconducting parameters, unequally contributing to hysteresis in different temperature ranges. Three parameters in Eq. (1), j_c, η, and u, depend on temperature. Their temperature dependences read as follows:

$$j_c = j_{c0}\left(1 - \frac{T}{T_c}\right), \tag{2}$$

$$\eta = \eta_0 \frac{1 - (T/T_c)^2}{1 + (T/T_c)^2}, \tag{3}$$

$$\frac{\langle u^2 \rangle}{a^2} = CT. \tag{4}$$

Here j_{c0} and η_0 are the critical current density and viscosity of the vortex matter at zero temperature, respectively, C is the constant varying for different materials. The above dependences are of empirical origin. Equation (2) represents the temperature dependence of the critical current density typical for ceramic HTSC.[27] This decreasing function of temperature reflects the fact of the reduction in the pinning strength with the temperature activation of vortices. The linear temperature dependence of j_c fits well the experimental data.

Vortex viscosity defines the dissipation of Copper pairs in the normal region of the vortex core originating upon vortex motion and can be analytically expressed as $\eta = \Phi_0 B_{c2}/\rho_n$ (Ref. 28) (Φ_0 is the magnetic flux quantum of 2.07 $\times 10^{-15}$ Wb and ρ_n is the normal-state resistivity). The temperature dependence of viscosity Eq. (3) is derived from an empirical relation for the upper critical field $B_{c2} = \Phi_0/2\pi\xi^2$ within the framework of the Ginsburg-Landau theory. It should be noted that this theory has shown its applicability for description of the upper critical field in pnictides.[29]

The equation for thermal fluctuations $\langle u^2 \rangle = 4\pi T\lambda^2/\Phi_0^{3/2}B^{1/2}$ (Ref. 30) was initially derived in the approximation of low temperatures, where $\lambda(T)$ has a weak dependence on temperature and only slightly differs from the value of $\lambda(0)$. Near T_c, the temperature dependence of $\lambda(T) = \lambda(0)[1-(T/T_c)^{1/4}]^{-1/2}$ has a divergence and account for this dependence yields nonphysical values for thermal fluctuations. When taking the ratio $\langle u^2 \rangle / \xi^2$ as in Refs. 2 and 31, the temperature dependence of penetration depth λ is compensated by that of the coherence length ξ and the ratio is directly proportional to temperature. In our case of the ratio $\langle u^2 \rangle / a^2$, the dependence $\lambda(T)$ is compensated by temperature changes in the mean distance a between pinning
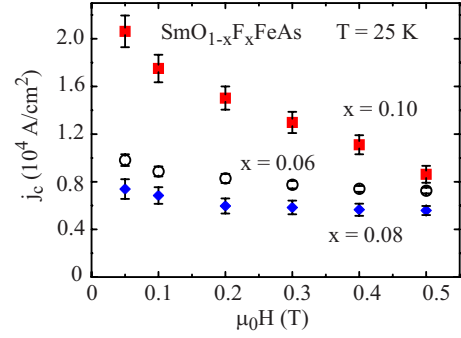

FIG. 9. (Color online) Magnetic field dependence of the critical current density j_c at T=25 K for SmO$_{1-x}$F$_x$FeAs samples with different fluorine doping: circles, x=0.06; diamonds, x=0.08; and squares, x=0.1.

centers. Namely, with increasing temperature, potential wells of shallow depth stop contributing to pinning and the "effective" distance between pinning centers increases. The linear temperature dependence of $\langle u^2 \rangle / a^2$ as suggested in Refs. 2 and 31 was used in our calculations. As can be seen in Fig. 8, the agreement between experimental data and theoretical curves is rather good. So our assumption of a linear temperature dependence of $\langle u^2 \rangle / a^2$ is appropriate. The influence of thermal fluctuations on the microwave absorption signal is as follows: under the action of thermal fluctuations, the position of a vortex in a potential well of a pinning center becomes an arbitrary value. Therefore, the phase of the absorption signal also becomes an arbitrary value and the amplitude of the fundamental harmonic decreases. The higher is the temperature, the greater is the misphasing of the MMA signal.

By substituting Eqs. (2)–(4) into Eq. (1), one may analyze the effect of each superconducting parameter on the temperature dependence of the MMA amplitude. Since the critical current density is a linear function of temperature for ceramic samples,[27] its effect leads to a gradual decrease in the hysteresis amplitude with increasing temperature up to T_c. The ratio ($\langle u^2 \rangle / a^2$) enters Eq. (1) exponentially, and as the amplitude of thermal fluctuations ($\langle u^2 \rangle$)$^{1/2}$ grows with temperature, the hysteresis amplitude $L(T)$ is significantly suppressed near T_c. Therefore, the only parameter, which can lead to the increase of the MMA amplitude near T_c, is the viscosity of the vortex matter η. This denotes that the local maximum observed for the SmO$_{0.9}$F$_{0.1}$FeAs sample results from competing effects of $\eta(T)$ and of $j_c(T)$ and $\langle u^2(T) \rangle$. Unfortunately, it is not possible to quantify the value of viscosity η, because this parameter explicitly enters the preexponential coefficient of Eq. (1), which, in turn, depends on the spectrometer settings (parameter A) that may vary for different sets of experiments. Nevertheless, qualitative examination of Eqs. (1)–(4) gives some insight into the processes contributing to the temperature behavior of the MMA hysteresis amplitude.

In order to find the magnetic field dependence of the critical current density, the procedure of fitting the theoretical curve $L(T,H$=const) to the experimental data was repeated at several values of the magnetic field. Figure 9 shows the critical current density calculated at T=25 K as a function of the magnetic field. The following tendency has been re-

vealed: the lower the concentration of fluorine in the sample is, the weaker appears the field dependence of the critical current density. This observation indicates that the samples with smaller fluorine concentration of 0.06 and 0.08 contain a larger number of pinning centers compared to the optimally doped sample with $x=0.1$. One can conjecture that nanoscale inclusions of a nonsuperconducting (possibly magnetic) phase might act as such centers. The nonmonotonous dependence of the critical current density on the fluorine content, i.e., that j_c for $SmO_{0.92}F_{0.08}FeAs$ is slightly smaller than that for $SmO_{0.94}F_{0.06}FeAs$, may be explained by the change in the ratio of sizes of nonsuperconducting inclusions and vortex cores. Apparently, the sizes of nonsuperconducting inclusions are maximal at the lowest fluorine concentration and shrink as doping tends to the optimal level. As a result, the effectiveness of pinning centers also decreases with increasing fluorine content.

The assumption of bigger nonsuperconducting inclusions at the lowest fluorine content is supported by estimates of the parameter $(\langle u^2\rangle/a^2)^{1/2}$. The ratio of the amplitude of thermal fluctuations $(\langle u^2\rangle)^{1/2}$ to the mean distance between pinning centers a has been obtained at $T=25$ K for the samples with fluorine content of 0.06, 0.08, and 0.1, respectively: $(\langle u^2\rangle/a^2)^{1/2}=0.36$, 0.16, and 0.19. Obviously u and a do not depend on the applied magnetic field. Indeed, the values of $(\langle u^2\rangle/a^2)^{1/2}$ obtained from the simulation at different values of the magnetic field scatter within the limits of calculation error (±0.03) only, which indicates the correct determination of this parameter by the simulation procedure. If the parameter $(\langle u^2\rangle)^{1/2}$ is not changing significantly with fluorine concentration, then the increase in the ratio $(\langle u^2\rangle/a^2)^{1/2}$ for the sample with minimal fluorine content, as compared with those for other samples, can be explained by a smaller distance between pinning centers, and as a result, either by a larger number of pinning centers or by their bigger sizes.

The stronger field dependence of the critical current density for the optimally doped sample ($x=0.1$) points to weaker pinning centers as compared to underdoped samples. A higher absolute value of the critical current density for this sample ($x=0.1$) is due to the higher critical temperature of the optimally doped sample.

V. CONCLUSION

A series of ceramic $SmO_{1-x}F_xFeAs$ samples with fluorine doping levels $x=0.06$, 0.08, and 0.1 was studied by the MMA method. A granular structure of the samples manifests itself in MMA and also ac susceptibility and resistivity measurements. However, the intergranular pinning is confined to the low-field regime, whereas the bulk intragranular pinning dominates at higher magnetic fields and defines the boundary of the irreversible and reversible behavior of magnetic characteristics of a superconductor. The superconducting parameters determined from MMA measurements both directly and by simulation reveal a strong pinning of vortices inside the grains in all samples. In particular, irreversibility lines are characterized with a steep ascent comparable with that of YBCO ceramics which is known to be a representative of the ReBa$_2$Cu$_3$O$_y$ class, possessing the highest pinning strength among HTSC cuprates. A theoretical analysis of MMA loops has enabled a quantitative estimate of the superconducting critical current density. Fluorine underdoped samples demonstrate weaker dependence of the critical current density on the magnetic field than an optimally doped sample. Such a remarkable effect may be due to the occurrence of nanoscale, possibly magnetic, nonsuperconducting inclusions coexisting with the superconducting phase, which serve as effective pinning centers for magnetic flux lines. This finding corroborates the growing evidence for the coexistence of the phases with competing order parameters in the underdoped Sm-based iron arsenide superconductor.

*npanarina@kfti.knc.ru

[1] Y. Kamihara, T. Watanabe, M. Hirano, and H. Hosono, J. Am. Chem. Soc. **130**, 3296 (2008).

[2] G. Blatter, M. V. Feigelman, V. B. Geshkenbein, A. I. Larkin, and V. M. Vinokur, Rev. Mod. Phys. **66**, 1125 (1994).

[3] Y. W. Ma, Z. S. Gao, L. Wang, Y. P. Qi, D. L. Wang, and X. P. Zhang, Chin. Phys. Lett. **26**, 037401 (2009).

[4] C. Hess, A. Kondrat, A. Narduzzo, J. E. Hamann-Borrero, R. Klingeler, J. Werner, G. Behr, and B. Büchner, EPL **87**, 17005 (2009).

[5] H. Luetkens, H.-H. Klauss, M. Kraken, F. J. Litterst, T. Dellmann, R. Klingeler, C. Hess, R. Khasanov, A. Amato, C. Baines, M. Kosmala, O. J. Schumann, M. Braden, J. Hamann-Borrero, N. Leps, A. Kondrat, G. Behr, J. Werner, and B. Büchner, Nature Mater. **8**, 305 (2009).

[6] L. Wang, U. Köhler, N. Leps, A. Kondrat, M. Nale, A. Gasparini, A. de Visser, G. Behr, C. Hess, R. Klingeler, and B. Büchner, Phys. Rev. B **80**, 094512 (2009).

[7] A. J. Drew, Ch. Niedermayer, P. J. Baker, F. L. Pratt, S. J. Blundell, T. Lancaster, R. H. Liu, G. Wu, X. H. Chen, I. Watanabe, V. K. Malik, A. Dubroka, M. Rössle, K. W. Kim, C. Baines, and C. Bernhard, Nature Mater. **8**, 310 (2009).

[8] F. J. Owens and C. P. Poole, Jr., *Electromagnetic Absorption in the Copper Oxide Superconductors* (Kluwer Academic, Dordrecht, 1999).

[9] A. Kondrat, J. E. Hamann-Borrero, N. Leps, M. Kosmala, O. Schumann, J. Werner, G. Behr, M. Braden, R. Klingeler, B. Büchner, and C. Hess, Eur. Phys. J. B **70**, 461 (2009).

[10] T. Shaposhnikova, Yu. Talanov, and Yu. Vashakidze, Physica C **385**, 383 (2003).

[11] C. P. Bean, Rev. Mod. Phys. **36**, 31 (1964).

[12] E. H. Brandt, Phys. Rev. B **54**, 4246 (1996).

[13] T. Wu, J. J. Ying, G. Wu, R. H. Liu, Y. He, H. Chen, X. F. Wang, Y. L. Xie, Y. J. Yan, and X. H. Chen, Phys. Rev. B **79**, 115121 (2009).

[14] S. Ruppel, G. Michels, H. Geus, J. Kalenborn, W. Schlabitz, B. Roden, and D. Wohlleben, Physica C **174**, 233 (1991).

[15] D. Wohlleben, G. Michels, and S. Ruppel, Physica C **174**, 242 (1991).

[16] V. Kataev, N. Knauf, B. Buchner, and D. Wohlleben, Physica C **184**, 165 (1991).

[17] M. Tinkham, *Introduction to Superconductivity*, 2nd ed. (McGraw-Hill, New York, 1996), p. 219.

[18] M. Pozek, A. Dulcic, and B. Rakvin, Physica C **169**, 95 (1990).

[19] M. Pozek, A. Dulcic, and B. Rakvin, Physica C **197**, 175 (1992).

[20] M. Muralidhar, N. Sakai, M. Jirsa, M. Murakami, and I. Hirabayashi, Appl. Phys. Lett. **92**, 162512 (2008).

[21] P. Rodrigues, Jr., J. Schaf, and P. Pureur, Phys. Rev. B **49**, 15292 (1994).

[22] X. Fan, M. Terasawa, T. Mitamura, T. Kohara, K. Ueda, H. Tsub-akino, K. Fukushima, and N. Takezawa, Physica C **282-287**, 2105 (1997).

[23] A. Schilling, R. Jin, J. D. Guo, and H. R. Ott, Phys. Rev. Lett. **71**, 1899 (1993).

[24] A. Narduzzo, M. S. Grbić, M. Požek, A. Dulčić, D. Paar, A. Kondrat, C. Hess, I. Hellmann, R. Klingeler, J. Werner, A. Kohler, G. Behr, and B. Büchner, Phys. Rev. B **78**, 012507 (2008).

[25] C. Kessler, B. Nebendahl, D.-N. Peligrad, A. Dulcic, H.-U. Habermeier, and M. Mehring, Physica C **219**, 233 (1994).

[26] T. Shaposhnikova, Yu. Vashakidze, R. Khasanov, and Yu. Talanov, Physica C **300**, 239 (1998).

[27] H. Darhmaoui and J. Jung, Phys. Rev. B **53**, 14621 (1996).

[28] J. Bardeen and M. J. Stephen, Phys. Rev. **140**, A1197 (1965).

[29] X. Zhu, H. Yang, L. Fang, G. Mu, and H.-H. Wen, Supercond. Sci. Technol. **21**, 105001 (2008).

[30] M. V. Feigel'man and V. M. Vinokur, Phys. Rev. B **41**, 8986 (1990).

[31] S. Patnaik, A. Gurevich, S. D. Bu, J. Choi, C. B. Eom, and D. C. Larbalestier, Phys. Rev. B **70**, 064503 (2004).